Optimal Power Flow Pursuit via Feedback-based Safe Gradient Flow

Antonin Colot*, Yiting Chen*, Bertrand Cornélusse, Jorge Cortés, and Emiliano Dall'Anese

***Abstract*—This paper considers the problem of controlling the operation of inverter-interfaced distributed energy resources (DERs) in a distribution grid, to achieve operational and performance goals with limited system-level information. We develop an online feedback optimization method to drive the DERs' power setpoints to solutions of an AC optimal power flow (OPF) problem based only on voltage measurements (and without requiring measurements of the power consumption of non-controllable assets). The proposed method – grounded on the theory of control barrier functions – is based on a continuous approximation of the projected gradient flow, appropriately modified to accommodate measurements from the power network. We provide results in terms of local exponential stability, and assess the robustness to errors in the measurements and in the system Jacobian matrix. We show that the proposed method ensures anytime satisfaction of the voltage constraints when no model and measurement errors are present; if these errors are present and are small, the voltage violation is practically negligible. We also discuss extensions of the framework to virtual power plant setups. Numerical experiments on a 93-bus distribution system and with realistic load and production profiles show a superior performance in terms of voltage regulation relative to existing methods.**

I. Introduction

This work seeks to contribute to the domain of real-time control and operation of distribution systems with high integration of inverter-interfaced distributed energy resources (DERs). The steady increase in energy costs, combined with government incentives advocating for the utilization of renewable energy sources and of energy-efficient automated load control, has reshaped the operation of distribution networks [1], [2]. Historically, distribution networks were designed to manage unidirectional power flows; however, the increased integration of renewable resources and load management strategies lead to operational and reliability challenges related to reversed power flows, voltage fluctuations, and power quality.

Traditional techniques based on solving an AC optimal power flow (OPF) problem [3], [4] require collecting information of all non-controllable powers and running an iterative method; this process may be long compared to the fast changing conditions of a modern distribution system [1], [2]; existing Volt/Var techniques may not fully resolve voltage regulation and may in fact increase line currents; recent works on emulating OPF solutions via neural networks can alleviate the computational burden [5], [6], but still require measurements of all the non-controllable powers (which are the inputs to the neural network), and may not even produce feasible power points. In this work, we focus on real-time AC OPF methods [7]–[12], and seek new strategies that exhibit strong performance in terms of achieved operational cost and voltage limit satisfaction (both from analytical and numerical standpoints), while using limited system information and measurements. In particular, we seek methods that do not require a complete AC model and knowledge of all the non-controllable powers throughout the nodes of the system.

Prior work. Several approaches have been explored to develop real-time OPF algorithms. In general, existing solutions leverage online optimization techniques, and incorporate measurements of some network quantities to bypass the need of a system-level model. In the following, we present a list that is by no means exhaustive. Feedback algorithms using voltage measurements based on linearized models were developed in [7], and recently [13] combined with data-driven learning to synthesize decentralized strategies; online primal-dual methods with voltage and/or power measurements have been proposed in [8], [14]; model-free counterparts were proposed in [15] and [16]. Discrete-time projected gradient algorithms for the OPF problem are employed in [11], [17], while projected gradient flows were used in [9]. Projection of gradient iterates onto a linearization of the feasible set around the current state was used in [12] for reactive power control. Power control for aggregations of DERs to track setpoints at the point of common coupling via gradient-type methods were proposed in, e.g., [18]. Online quasi-Newton methods were used in [19], and online interior-point methods were proposed in [20]. In addition to [7], distributed methods were explored in, e.g., [21].

Contributions. Our contributions are as follows.
(c1) We propose a new approach for the design of real-time OPF algorithms that is grounded on the theory of control barrier functions (CBFs) [22]. We leverage a continuous approximation of projected gradient flows [23], appropriately modified to accommodate voltage measurements from the power network. Inheriting the properties of CBF methods, the proposed algorithm – here termed feedback-based safe gradient flow (SGF) – ensures anytime satisfaction of the voltage constraints, while reaching solutions of the OPF.
(c2) From a theoretical standpoint, we show that the proposed feedback-based SGF renders isolated optimal solutions of the AC OPF problem locally exponentially stable and ensures the anytime satisfaction of the voltage constraints. Moreover, wye

* Equal contribution of the authors. Y. Chen and E. Dall'Anese are with the Department of Electrical, Computer, and Energy Engineering, University of Colorado Boulder; A. Colot is a Research Fellow of the Fonds de la Recherche Scientifique with the Montefiore Institute, University of Liège, and a visiting student at the University of Colorado Boulder; B. Cornélusse is with the Montefiore Institute, University of Liège; J. Cortés is with the Department of Mechanical and Aerospace Engineering, University of California, San Diego.

This work was supported in part by the National Science Foundation (NSF) awards 1941896 and 1947050.

provide practical exponential stability results when voltage measurements are affected by errors and when the Jacobian matrix of the AC power flow equations is computed only approximately. In this case, if errors are small, the voltage violation is practically negligible.

(c3) We perform numerical experiments on a 93-bus distribution system [24] and with realistic load and solar production profiles from the Open Power System Data. We show that our method shows far superior performance in terms of voltage regulation relative to existing online primal-dual methods and Volt/Var strategies.

We note that, relative to [12], our design leverages the theory of CBFs [22], [23], our method can handle constraints that are nonlinear, and we provide practical stability and forward-invariance guarantees.

II. Problem formulation

A. Distribution system model

Consider an electrical distribution system[1] with $N+1$ nodes and hosting G distributed energy resources (DERs); these may include inverter-interfaced photovoltaic systems, energy storage systems, variable-speed drives, and electric vehicles, or small-scale generators if any. The node 0 is taken to be the substation or the point of common coupling, while $\mathcal{N} := \{1, ..., N\}$ is the set of remaining nodes. We consider a steady-state model where voltages and currents are represented in the phasor domain. Accordingly, let $v_k = \nu_k e^{j\delta_k} \in \mathbb{C}$, $\nu_k := |v_k|$, and $i_k = |i_k| e^{j\psi_k} \in \mathbb{C}$ the line-to-ground voltage and current injected at node i, respectively. Moreover, the voltage at node 0 is set to $v_0 = V_0 e^{j\delta_0}$ [25].

Using Ohm's Law and Kirchoff's Law, one has the usual phasor relationship:

$$\begin{bmatrix} i_0 \\ \boldsymbol{i} \end{bmatrix} = \begin{bmatrix} y_0 & \bar{\boldsymbol{y}}^T \\ \bar{\boldsymbol{y}} & \boldsymbol{Y} \end{bmatrix} \begin{bmatrix} v_0 \\ \boldsymbol{v} \end{bmatrix} \tag{1}$$

where $\boldsymbol{v} \in \mathbb{C}^N$ collects the voltages $\{v_k\}_{k\in\mathcal{N}}$, $\boldsymbol{i} \in \mathbb{C}^N$ collects the currents $\{i_k\}_{k\in\mathcal{N}}$, and $\boldsymbol{Y} \in \mathbb{C}^{N\times N}$, $\bar{\boldsymbol{y}} \in \mathbb{C}^N$, and $y_0 \in \mathbb{C}$ are based on the admittances of the distribution lines; see, for example, [25], [26]. Using (1), it is possible to relate complex powers at the nodes $\mathcal{N}$ with voltages as

$$\boldsymbol{s} = \text{diag}(\boldsymbol{v}) \left(\bar{\boldsymbol{y}}^* v_0^* + \boldsymbol{Y}^* \boldsymbol{v}^*\right) \tag{2}$$

where $\boldsymbol{s} = \boldsymbol{p}_{\text{net}} + \text{j}\boldsymbol{q}_{\text{net}} \in \mathbb{C}^N$, with $\boldsymbol{p}_{\text{net}}$ and $\boldsymbol{q}_{\text{net}}$ vectors collecting the net active and reactive power injections at nodes $\mathcal{N}$. Note that $\boldsymbol{p}_{\text{net}}$ and $\boldsymbol{q}_{\text{net}}$ account for both the powers (injected or consumed) of the DERs and the aggregate powers of the non-controllable loads that are connected to each of the nodes $\mathcal{N}$. In particular, let $\boldsymbol{p}_l := [p_{l,1}, \ldots, p_{l,N}]^\top \in \mathcal{W}_p$, $\boldsymbol{q}_l := [q_{l,1}, \ldots, q_{l,N}]^\top \in \mathcal{W}_q$ with a compact sets $\mathcal{W}_p \subset \mathbb{R}^N$ and $\mathcal{W}_q \subset \mathbb{R}^N$, be vectors collecting the net active and reactive power consumed at the nodes by non-controllable devices (positive when the power is consumed). For the G DERs, consider the vector $\boldsymbol{u} = [p_1, p_2, ..., p_G, q_1, q_2, ..., q_G]^\top$ collecting their active and reactive powers (with a positive sign denoting generation). Moreover, let $\mathcal{G} := \{1, ..., G\}$ be the index for the DERs, and define a function $m : \mathcal{G} \to \mathcal{N}$ which maps a DER index to the node where the DER is connected to. With this notation, note that $\mathcal{G}_n := \{i \in \mathcal{G} : n = m(i)\}$ is the set of DERs connected at node $n \in \mathcal{N}$. Then, the net active and reactive powers are given by $p_{\text{net},n} = \sum_{j\in\mathcal{G}_n} p_j - p_{l,n}$ and $q_{\text{net},n} = \sum_{j\in\mathcal{G}_n} q_j - q_{l,n}$ at each n. In what follows, we consider a set of nodes $\mathcal{M} \subseteq \mathcal{N}$ with cardinality $M = |\mathcal{M}|$ where voltages are to be regulated (if the operator would like to monitor and regulate all the voltages, then $\mathcal{M} = \mathcal{N}$).

Based on the Implicit Function Theorem and the results of, e.g., [26], [27], we make the following assumption on (2).

Assumption 1 (*Mapping*)**.** *There exists a unique continuously differentiable function $H : \mathbb{R}^{2G} \times \mathcal{W}_p \times \mathcal{W}_q \to \mathbb{R}^M$ such that, $H_i(\boldsymbol{u}; \boldsymbol{p}_l, \boldsymbol{q}_l) = \nu_i = |v_i|$, for $i \in \mathcal{M}$. The Jacobian $J_h(\boldsymbol{u}) := \frac{\partial H(\boldsymbol{u};\boldsymbol{p}_l,\boldsymbol{q}_l)}{\partial \boldsymbol{u}}$ is locally Lipschitz continuous.* □

This relationship is typically used in optimization problems such as the AC OPF [3], [4].

Remark II.1 (*Model and notation*)**.** It is important to note that the framework proposed in this paper is for multi-phase distribution systems with both wye and delta connections (similar to, e.g., [8], [14]); however, to simplify the notation and to streamline the exposition, we outline the framework using a balanced model. □

B. OPF for distribution systems

In this section, we outline a formulation of the OPF problem for distribution systems. By solving an OPF problem, one seeks power setpoints for the DERs that minimize the operational cost (or maximize performance objectives) for the utilities and the customers, subject to operational constraints that may include voltage limits, line ampacity, or hardware limits [3], [4]. The cost associated with the utility companies may favor the minimization of system losses or the usage of controllable resources, or may perform voltage regulation (e.g., thus including cost of active power curtailment or reactive power compensation [7], [21]); on the other hand, customers may want to minimize the power curtailed by renewables or maximize their revenue by providing ancillary services.

To outline our framework, we start with the following formulation of the OPF problem (we present some extensions later in Section III-C):

$$\begin{aligned} \min_{\boldsymbol{\nu}\in\mathbb{R}^M, \boldsymbol{u}\in\mathbb{R}^{2G}} \quad & C_v(\boldsymbol{\nu}) + C_p(\boldsymbol{u}) & \\ \text{s.t.} \quad & \underline{V} \le \nu_i \le \bar{V} & \forall i \in \mathcal{M} \\ & \nu_i = H_i(\boldsymbol{u}; \boldsymbol{p}_l, \boldsymbol{q}_l) & \forall i \in \mathcal{M} \\ & (p_i, q_i) \in \mathcal{U}_i & \forall i \in \mathcal{G} \end{aligned} \tag{3}$$

where the functions $C_v : \mathbb{R}^M \to \mathbb{R}$ and $C_p : \mathbb{R}^{2G} \to \mathbb{R}$ have locally Lipschitz continuous gradients, $\underline{V}$ and $\bar{V}$ are predefined voltage bounds that the operator wants to enforce at nodes $i \in \mathcal{M}$, $H_i(\boldsymbol{u}; \boldsymbol{p}_l, \boldsymbol{q}_l)$ is the ith component of the function $H(\boldsymbol{u}; \boldsymbol{p}_l, \boldsymbol{q}_l)$ (specifying the voltage magnitude ν_i), and $\mathcal{U}_i \subset$

[1]Upper-case (lower-case) boldface letters are used for matrices (column vectors); $(.)^\top$ denotes the transposition and $(.)^*$ the complex-conjugate; j the imaginary unit and $|.|$ the absolute value of a number. If we consider a given vector $\boldsymbol{x} \in \mathbb{R}^N$, diag$(\cdot)$ returns a $N \times N$ matrix with the element of $\boldsymbol{x}$ in its diagonal. For vectors $x \in \mathbb{R}^n$ and $u \in \mathbb{R}^m$, $\|x\|$ denotes the ℓ_2-norm and $(x, u) \in \mathbb{R}^{n+m}$ denotes their vector concatenation. We denote as $\mathbb{0}$ a vector or matriz with all zeros (the dimentiosn will be clear from the context).

$\mathbb{R}^2$ is a compact set of admissible power setpoints for the ith DER. We note that (3) can be equivalently re-written as:

$$\begin{aligned} \min_{\boldsymbol{u}\in\mathbb{R}^{2G}} \quad & C_v(H(\boldsymbol{u};\boldsymbol{p}_l,\boldsymbol{q}_l)) + C_p(\boldsymbol{u}) \\ \text{s.t.} \quad & \underline{V} \le H_i(\boldsymbol{u};\boldsymbol{p}_l,\boldsymbol{q}_l) \le \bar{V} \quad \forall i \in \mathcal{M} \\ & (p_i,q_i) \in \mathcal{U}_i \qquad\qquad\quad \forall i \in \mathcal{G} \end{aligned} \tag{4}$$

where $\boldsymbol{u}$ is the only optimization variable. Hereafter, we assume the set $\mathcal{U}_i$ can be expressed as

$$\mathcal{U}_i = \{(p_i,q_i) \in \mathbb{R}^2 : \ell_i(p_i,q_i) \le \mathbb{0}_{n_{c_i}}\} \tag{5}$$

where $\ell_i : \mathbb{R}^2 \to \mathbb{R}^{n_{c_i}}$ is a vector-valued function modeling power limits, and the inequality is taken entry-wise. For example, if the ith DER is an inverter-interfaced controllable renewable source, then $\ell_i(p_i,q_i) = [p_i^2+q_i^2-s_{n,i}^2, p_i-p_{\max,i}, -p_i]^\top$, where $s_{n,i}$ and $p_{\max,i}$ denote the inverter rated size and the maximum available active power, respectively; that is, $\mathcal{U}_i = \{(p_i,q_i) \in \mathbb{R} : p_i^2+q_i^2 \le s_{n,i}^2, p_i \le p_{\max,i}, p_i \ge 0\}$. Moreover, we define $\mathcal{U} := \mathcal{U}_1 \times \mathcal{U}_2 \times \ldots \times \mathcal{U}_G$ and denote as

$$\mathcal{F} := \{\boldsymbol{u} : \underline{V} \le H_i(\boldsymbol{u};\boldsymbol{p}_l,\boldsymbol{q}_l) \le \bar{V}, \forall i \in \mathcal{M}, \boldsymbol{u} \in \mathcal{U}\} \tag{6}$$

the feasible set of (4). We impose the following assumption on (4), which is typical in the AC OPF context.

Assumption 2 (Regularity of isolated solutions)**.** *Assume that* (4) *is feasible and let $\boldsymbol{u}^*$ be a local minimizer and an isolated Karush–Kuhn–Tucker (KKT) point for* (4)*, for given $\boldsymbol{p}_l, \boldsymbol{q}_l$. Assume that the following hold:*
i) Strict complementarity condition [28] and the linear independence constraint qualification (LICQ) hold at $\boldsymbol{u}^*$.
ii) The maps $\boldsymbol{u} \mapsto C_p(\boldsymbol{u})$, $\boldsymbol{u} \mapsto C_v(H(\boldsymbol{u};\boldsymbol{p}_l,\boldsymbol{q}_l))$ and $\boldsymbol{u} \mapsto H(\boldsymbol{u};\boldsymbol{p}_l,\boldsymbol{q}_l)$ are twice continuously differentiable over some open neighborhood $\mathcal{B}(\boldsymbol{u}^*, r_1) := \{\boldsymbol{u} : \|\boldsymbol{u}-\boldsymbol{u}^*\| < r_1\}$ of $\boldsymbol{u}^*$, and their Hessian matrices are positive semi-definite at $\boldsymbol{u}^*$.
iii) The Hessian $\nabla^2 C_p(\boldsymbol{u}^*)$ is positive definite. □

Assumption 2 imposes some mild regularity assumptions on a neighborhood of a strict locally optimal solution [29]; we note that, if (4) is formulated based on the linearized AC power flow equations [7], [8] and the cost is strongly convex, then Assumption 2 is satisfied.

Problem (4) can be solved using traditional optimization methods for nonlinear programs. However, *(c1)* these batch methods require collecting measurements of all the *non-controllable* powers $\boldsymbol{p}_l, \boldsymbol{q}_l$; moreover, *(c2)* the time required to collect the measurements of the non-controllable powers and run an iterative method to convergence may be long compared to the fast changing conditions of a modern distribution system [1], [2]. Although recent work on neural networks for AC OPF can alleviate the computational burden (see, e.g., the representative works [5], [6]), they still require measurements of all the non-controllable powers $\boldsymbol{p}_l, \boldsymbol{q}_l$ as in *(c1)*, and they often times rely on heuristics to return a feasible solution. Motivated by the challenges *(c1)–(c2)* and by the need to generate power setpoints that ensure satisfaction of voltage limits even under uncertain and time-varying operational setups, in this paper we seek to solve to the following problem.

Problem 1. *Design an online feedback optimization method that drives the DERs' power setpoints $\boldsymbol{u}$ to solutions of the problem* (4)*, while ensuring that voltage constraints are always met. The feedback optimization method should use measurements of the voltages instead of requiring knowledge of the non-controllable powers $\boldsymbol{p}_l, \boldsymbol{q}_l$.* □

We note that in Problem 1 we focus on voltage measurements because (4) includes voltage constraints; if (4) is modified to include cost and constraints associated with power flows or currents, then the feedback optimization method would require measurements of those quantities too [14].

III. Safe OPF pursuit

A. Feedback-based online algorithm

To solve our regulation problem, we propose the following feedback-based algorithm:

$$\dot{\boldsymbol{u}} = \eta F_\beta(\boldsymbol{u}, \tilde{\boldsymbol{\nu}}) \tag{7}$$

$$\begin{aligned} F_\beta(\boldsymbol{u},\tilde{\boldsymbol{\nu}}) := \arg\min_{\boldsymbol{\theta}\in\mathbb{R}^{2G}} \ & \|\boldsymbol{\theta} + \nabla C_p(\boldsymbol{u}) + J_H(\boldsymbol{u})^\top \nabla C_v(\tilde{\boldsymbol{\nu}})\|^2 \\ \text{s.t.} \ & -\nabla H_i(\boldsymbol{u})^\top \boldsymbol{\theta} \le -\beta\,(\underline{V} - \tilde{\nu}_i) \ \ \forall i \in \mathcal{M} \\ & \nabla H_i(\boldsymbol{u})^\top \boldsymbol{\theta} \le -\beta\,(\tilde{\nu}_i - \bar{V}) \ \ \forall i \in \mathcal{M} \\ & J_{\ell_i}(\boldsymbol{u})^\top \boldsymbol{\theta} \le -\beta \ell_i(p_i,q_i) \qquad \forall i \in \mathcal{G} \end{aligned} \tag{8}$$

where $\tilde{\nu}_i$ is a measurement of $|v_i|$ at node i, $J_H(\boldsymbol{u})$ is the Jacobian matrix of $H(\boldsymbol{u};\boldsymbol{p}_l,\boldsymbol{q}_l)$, $\nabla H_i(\boldsymbol{u}) = [\{(J_H(\boldsymbol{u}))_{i,j}\}_{j\in\mathcal{G}}]^\top$ is a $2G \times 1$ vector collecting the entries of $J_H(\boldsymbol{u})$ in the ith row and columns corresponding to nodes in $\mathcal{G}$, $J_{\ell_i}(p_i,q_i)$ is the Jacobian of $(p_i,q_i) \mapsto \ell_i(p_i,q_i)$, $\beta > 0$ is a design parameter, and $\eta > 0$ is the controller gain. For given $\boldsymbol{u}$ and $\tilde{\boldsymbol{\nu}}$, problem (8) is a convex quadratic program (QP) with a strongly convex cost; it can be efficiently solved using standard or high-performance embedded solvers for QPs, e.g., [30].

The online feedback optimization algorithm (7) is inspired by CBFs methods [22] and the safe gradient flow in [23]; we provide more details on the CBF-based design in Appendix A. In particular, (7) is an approximation of the projected gradient flow $\dot{\boldsymbol{u}} = \text{proj}_{T_\mathcal{F}(\boldsymbol{u})}\{-\nabla C_p(\boldsymbol{u}) - J_H^\top \nabla C_v(H(\boldsymbol{u};\boldsymbol{p}_l,\boldsymbol{q}_l))\}$, where $T_\mathcal{F}(\boldsymbol{u})$ is the tangent cone of $\mathcal{F}(\boldsymbol{u})$ at $\boldsymbol{u}$; in fact, one can show [23, Prop. 4.4] that $\lim_{\beta\to\infty} F_\beta(\boldsymbol{u}, H(\boldsymbol{u};\boldsymbol{p}_l,\boldsymbol{q}_l)) = \text{proj}_{T_\mathcal{F}(\boldsymbol{u})}\{-\nabla C_p(\boldsymbol{u}) - J_H^\top \nabla C_v(H(\boldsymbol{u};\boldsymbol{p}_l,\boldsymbol{q}_l))\}$.

The algorithm (7) is designed to steer the power setpoints of the DERs $\boldsymbol{u}$ to optimal solutions of the AC OPF, while continuously guaranteeing feasibility (i.e., satisfaction of voltage limits). As shown in Figure 1, (7) effectively acts as a feedback controller by replacing the voltage *model* $H(\boldsymbol{u};\boldsymbol{p}_l,\boldsymbol{q}_l)$ with *measurements* $\tilde{\boldsymbol{\nu}}$ of the voltage magnitudes. This is a key modification that allows one to avoid collecting measurements of $\boldsymbol{p}_l, \boldsymbol{q}_l$ [7], [8], [14]. However, we note that (7) requires the computation of the Jacobian matrix of $H(\boldsymbol{u};\boldsymbol{p}_l,\boldsymbol{q}_l)$. When this is not possible, we modify it as follows:

$$\dot{\boldsymbol{u}} = \eta \hat{F}_\beta(\boldsymbol{u}, \tilde{\boldsymbol{\nu}}) \tag{9}$$

$$\begin{aligned} \hat{F}_\beta(\boldsymbol{u},\tilde{\boldsymbol{\nu}}) := \arg\min_{\boldsymbol{\theta}\in\mathbb{R}^{2G}} \ & \|\boldsymbol{\theta} + \nabla C_p(\boldsymbol{u}) + J_{\hat{H}}^\top \nabla C_v(\tilde{\boldsymbol{\nu}})\|^2 \\ \text{s.t.} \ & -\nabla \hat{H}_i(\boldsymbol{u})^\top \boldsymbol{\theta} \le -\beta\,(\underline{V} - \tilde{\nu}_i) \ \ \forall i \in \mathcal{M} \\ & \nabla \hat{H}_i(\boldsymbol{u})^\top \boldsymbol{\theta} \le -\beta\,(\tilde{\nu}_i - \bar{V}) \ \ \forall i \in \mathcal{M} \\ & J_{\ell_i}(\boldsymbol{u})^\top \theta \le -\beta \ell_i(p_i,q_i) \qquad \forall i \in \mathcal{G} \end{aligned} \tag{10}$$

where $J_{\hat{H}}$ and $\{\hat{H}_i\}_{i\in\mathcal{M}}$ are computed based on a linear approximation of the AC power flow equations of the form

$$\hat{H}_n(\boldsymbol{u};\boldsymbol{p}_l,\boldsymbol{q}_l) = \sum_{i\in\mathcal{G}}(r_{n,m(i)}p_i + b_{n,m(i)}q_i) + c_n(\boldsymbol{p}_l,\boldsymbol{q}_l) \quad (11)$$

$n \in \mathcal{N}$, where the coefficients $\{r_{n,m(i)}, b_{n,m(i)}\}_{i\in\mathcal{G}}$ can be found as explained in e.g., [7], [26], [27], [31]. Effectively, the approximate Jacobian $\hat{J}_{\hat{H}}$ no longer depends on $\boldsymbol{u}$ and the non-controllable powers $\boldsymbol{p}_l, \boldsymbol{q}_l$; accordingly, it does not need to be re-computed when running (9).

The proposed feedback-based SGF is summarized in Algorithm 1 and illustrated in Fig. 1.

Algorithm 1 *Feedback-based safe gradient flow*

Initialization: Compute $J_{\hat{H}}$ and $\{\hat{H}_i, i \in \mathcal{M}\}$. Set $\beta > 0$, $\eta > 0$.

Real-time operation: for $t \geq 0$

[S1a] Measure power setpoints $\{p_i(t), q_i(t), i \in \mathcal{G}\}$

[S1b] Measure voltages $\{\tilde{\nu}_i(t), i \in \mathcal{M}\}$

[S2a] Update power setpoints via $\dot{\boldsymbol{u}}(t) = \eta\hat{F}_\beta(\boldsymbol{u}(t), \tilde{\boldsymbol{\nu}}(t))$

[S2b] Implement setpoints $\boldsymbol{u}(t)$

Remark III.1 (*Pseudo-measurements*)**.** The safe gradient flow (9) relies on measurements of the voltages at the network locations $\mathcal{M}$. However, the system operator may utilize a mix of actual voltage measurements and pseudo-measurements [32]. For example, suppose that the system operator can measure voltages at some nodes $\mathcal{M}_{\text{meter}} \subset \mathcal{M}$ and relies on pseudo-measurements at the other nodes. Then,

$$\tilde{\nu}_i = \begin{cases} H_i(\boldsymbol{u};\boldsymbol{p}_l,\boldsymbol{q}_l) + n_i, & i \in \mathcal{M}_{\text{meter}} \\ H_{i,\text{pseudo}}(\boldsymbol{u};\boldsymbol{p}_l,\boldsymbol{q}_l), & i \in \mathcal{M}\setminus\mathcal{M}_{\text{meter}} \end{cases} \quad (12)$$

where n is a bounded measurement noise, and $H_{i,\text{pseudo}}(\boldsymbol{u};\boldsymbol{p}_l,\boldsymbol{q}_l)$ represent a model used to generate the pseudo-measurements (i.e., a power flow solver). □

Remark III.2 (*Measurement of setpoints*)**.** If the embedded controllers of inverters are guaranteed to implement the power setpoints, in principle, the step [S1a] in Algorithm 1 is not needed. However, the operator may want to measure current setpoints $\{p_i(t), q_i(t), i \in \mathcal{G}\}$ for verification purposes and to monitor the state of the DERs' inverters. □

In the next section, we analyze the convergence and stability properties of the proposed feedbck-based SGF (9).

B. Stability analysis and constraint satisfaction guarantees

In our technical analysis, we make use of the following assumptions. The assumptions are stated for a given values of the non-controllable powers $\boldsymbol{p}_l, \boldsymbol{q}_l$.

Assumption 3 (*Jacobian errors*)**.** *$\exists\ E_h < +\infty, E_J < +\infty$ such that $\|\hat{H}(\boldsymbol{u};\boldsymbol{p}_l,\boldsymbol{q}_l) - H(\boldsymbol{u};\boldsymbol{p}_l,\boldsymbol{q}_l)\| \leq E_h$ and $\|J_{\hat{H}}(\boldsymbol{u}) - J_H(\boldsymbol{u})\| \leq E_J$ for any $\boldsymbol{u} \in \mathcal{B}(\boldsymbol{u}^*, r_1)$.* □

Assumption 4 (*Measurement errors*)**.** *$\exists\ E_M < +\infty$ such that $\|\tilde{\boldsymbol{\nu}} - \boldsymbol{\nu}\| \leq E_M$.* □

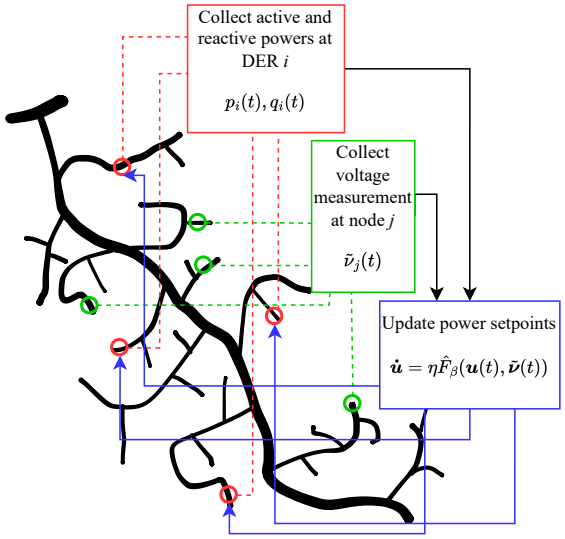

Fig. 1: Closed-loop implementation of the proposed online feedback optimization algorithm. The proposed scheme leverages measurements of voltages and pseudo-measurements (if available) to solve the AC OPF problem (4).

Assumptions 3-4 are motivated by the following observations: (i) the linear map error $\|\hat{H}(\boldsymbol{u};\boldsymbol{p}_l,\boldsymbol{q}_l) - H(\boldsymbol{u};\boldsymbol{p}_l,\boldsymbol{q}_l)\|$ is bounded and small in a neighborhood of the optimizer (as confirmed in Fig. 3f in our numerical results), and (ii) in realistic monitoring and SCADA systems, the measurement of the voltage magnitudes are affected by a small (or even negligible) error.

In our analysis, we view (9) as a perturbed version of (7). To begin with, we have the following result.

Lemma III.3 (*KKT and equilibrium*)**.** *Consider the problem* (4) *satisfying Assumptions 1-2. There exists $\boldsymbol{\mu}^*$ such that $(\boldsymbol{u}^*, \boldsymbol{\mu}^*)$ is a KKT point for* (4) *if and only if $\boldsymbol{u}^*$ is an equilibrium of $\dot{\boldsymbol{u}} = \eta F_\beta(\boldsymbol{u}, H(\boldsymbol{u};\boldsymbol{p}_l,\boldsymbol{q}_l))$.* □

Before analyzing the stability of the proposed feedback-based SGF, we provide some notation and intermediate results that will be used in the proof of our main result.

Let $\Omega := J_{\hat{H}}(\boldsymbol{u}) - J_H(\boldsymbol{u})$ and denote by ω_i the i-th row of Ω. Moreover, let $\mathbf{e} := \tilde{\boldsymbol{\nu}} - \boldsymbol{\nu}$ denote the measurement errors. Then, define $\bar{F}_\beta(\boldsymbol{u}, \Omega, \mathbf{e})$ as

$$\begin{aligned} &\bar{F}_\beta(\boldsymbol{u}, \Omega, \mathbf{e}) \\ &:= \arg\min_{\boldsymbol{\theta}} \|\boldsymbol{\theta} + \nabla C_p(\boldsymbol{u}) + (J_H(\boldsymbol{u}) + \Omega)^\top \nabla C_v(\boldsymbol{\nu} + \mathbf{e})\|^2 \\ &\quad \text{s.t.} -(\nabla H_i(\boldsymbol{u}) + \omega_i)^\top \boldsymbol{\theta} \leq -\beta\,(\underline{V} - \nu_i - e_i) \quad \forall i \in \mathcal{M} \\ &\qquad (\nabla H_i(\boldsymbol{u}) + \omega_i)^\top \boldsymbol{\theta} \leq -\beta\,(\nu_i + e_i - \bar{V}) \quad \forall i \in \mathcal{M} \\ &\qquad J_{\ell_i}(\boldsymbol{u})^\top \theta \leq -\beta\ell_i(p_i, q_i) \qquad \forall i \in \mathcal{G} \end{aligned}$$

where $\boldsymbol{\nu} = H(\boldsymbol{u};\boldsymbol{p}_l,\boldsymbol{q}_l)$. Note that $F_\beta(\boldsymbol{u}, H(\boldsymbol{u};\boldsymbol{p}_l,\boldsymbol{q}_l)) = \bar{F}_\beta(\boldsymbol{u}, \mathbb{0}, \mathbb{0})$ and $\hat{F}_\beta(\boldsymbol{u}, \tilde{\boldsymbol{\nu}}) = \bar{F}_\beta(\boldsymbol{u}, J_{\hat{H}}(\boldsymbol{u}) - J_H(\boldsymbol{u}), \tilde{\boldsymbol{\nu}} - \boldsymbol{\nu})$. Let $\mathcal{E}_J := \{\Omega : \|\Omega\| \leq E_J\}$ and $\mathcal{E}_M := \{\mathbf{e} : \|\mathbf{e}\| \leq E_M\}$ for brevity. We make the following assumption on $\bar{F}_\beta$.

Assumption 5 (*Regularity*)**.** *For any $\boldsymbol{u} \in \mathcal{B}(\boldsymbol{u}^*, r_1)$, and any Ω and $\mathbf{e}$ satisfying Assumptions 3-4, the problem* (10) *is feasible, and satisfies the Mangasarian-Fromovitz Constraint Qualification and the constant-rank condition [33].* □

Since the constraints in the problem defining $\bar{F}_\beta(\boldsymbol{u}, \Omega, \mathbf{e})$

(and, hence, our safe gradient flow (9)) are based on techniques from CBFs [22], [23], Assumption 5 guarantees that there always exists a direction for the setpoints to satisfy the constraints of the OPF. Moreover, this assumption allows us to derive the following result.

Lemma III.4 (*Lipschitz continuity*)**.** *Let Assumption 5 hold, and assume that* $\boldsymbol{u} \mapsto C_p(\boldsymbol{u})$, $\boldsymbol{\nu} \mapsto C_v(\boldsymbol{\nu})$ *are twice continuously differentiable over* $\mathcal{B}(\boldsymbol{u}^*, r_1)$ *and* $\mathcal{V} := \{\boldsymbol{\nu} \in \mathbb{R}^M : \underline{V} \leq \nu_i + e_i \leq \bar{V}, \forall i \in \mathcal{M}, \boldsymbol{\nu} = H(\boldsymbol{u}; \boldsymbol{p}_l, \boldsymbol{q}_l), \|\mathbf{e}\| \leq E_M, \boldsymbol{u} \in \mathcal{B}(\boldsymbol{u}^*, r_1)\}$*, respectively. Then:*
(i) For any $\Omega \in \mathcal{E}_J$ *and* $\mathbf{e} \in \mathcal{E}_M$, $\boldsymbol{u} \mapsto \bar{F}_\beta(\boldsymbol{u}, \Omega, \mathbf{e})$ *is locally Lipschitz at* $\boldsymbol{u}$, $\boldsymbol{u} \in \mathcal{B}(\boldsymbol{u}^*, r_1)$.
(ii) For any $\boldsymbol{u} \in \mathcal{B}(\boldsymbol{u}^*, r_1)$ *and* $\Omega \in \mathcal{E}_J$, $\mathbf{e} \mapsto \bar{F}_\beta(\boldsymbol{u}, \Omega, \mathbf{e})$ *is Lipschitz with constant* $\ell_{F_v} \geq 0$ *over* $\mathcal{E}_M$.
(iii) For any $\boldsymbol{u} \in \mathcal{B}(\boldsymbol{u}^*, r_1)$ *and* $\mathbf{e} \in \mathcal{E}_M$, $\Omega \mapsto \bar{F}_\beta(\boldsymbol{u}, \boldsymbol{\nu}, \Omega, \mathbf{e})$ *is Lipschitz with constant* $\ell_{F_J} \geq 0$ *over* $\mathcal{E}_J$. □

Lemma III.4 follows from [33, Theorem 3.6], and by the compactness of the sets $\mathcal{E}_M$ and $\mathcal{E}_J$. This result ensures existence and uniqueness of solutions for the proposed feedback-based safe gradient flow [34, Ch. 3].

Our main stability result critically relies on these results. Before stating it, we introduce some useful quantities that play a role in the main result; in particular, they are related to local properties of $F_\beta(\boldsymbol{u}, H(\boldsymbol{u}; \boldsymbol{p}_l, \boldsymbol{q}_l))$. Recall that $\boldsymbol{u}^*$ is the local optimizer of (4). We define $\boldsymbol{\nu}^* := H(\boldsymbol{u}^*; \boldsymbol{p}_l, \boldsymbol{q}_l)$, $E := \frac{\partial \bar{F}_\beta(\boldsymbol{u}, H(\boldsymbol{u}; \boldsymbol{p}_l, \boldsymbol{q}_l))}{\partial \boldsymbol{u}} \mid_{\boldsymbol{u}=\boldsymbol{u}^*}$, $e_1 := -\lambda_{\max}(E)$, and $e_2 := -\lambda_{\min}(E)$. Then, we can write the dynamics as $F_\beta(\boldsymbol{u}, H(\boldsymbol{u}; \boldsymbol{p}_l, \boldsymbol{q}_l)) = E(\boldsymbol{u} - \boldsymbol{u}^*) + \hat{g}(\boldsymbol{u})$, where $\hat{g}(u)$ satisfies $\|\hat{g}(\boldsymbol{u})\| \leq L\|\boldsymbol{u} - \boldsymbol{u}^*\|^2$, $\forall \boldsymbol{u} \in \mathcal{B}(\boldsymbol{u}^*, r_2)$, for some $L > 0$ and $r_2 > 0$ (see [34]). Define $r := \min\{r_1, r_2\}$ and

$$s_{\min} := \begin{cases} 0, & \text{if } r \geq \frac{e_1}{L}, \\ 1 - \frac{rL}{e_1}, & \text{if } r < \frac{e_1}{L}. \end{cases}$$

Since $\mathcal{U}$ is compact, $J_H(\boldsymbol{u})$ is Lipschitz on $\mathcal{U}$. We denote by ℓ_H its Lispchitz constant on $\mathcal{U}$. We are now ready to state the main stability result for (9).

Theorem III.5 (*Practical local exponential stability*)**.** *Consider the OPF problem* (4) *satisfying Assumptions 1-2, a linear map* $\hat{H}$ *satisfying Assumption 3, measurements* $\tilde{\boldsymbol{\nu}}$ *satisfying Assumption 4, and the controller* (9) *satisfying Assumption 5. Let* $\boldsymbol{u}(t)$, $t \geq t_0$, *be the unique trajectory of* (9)*. Assume that the set* $\mathcal{S} := \left\{s : s_{\min} < s \leq 1,\ e_1^{-3} e_2 L(\ell_{F_J} E_J + \ell_{F_v} E_M) < s - s^2\right\}$ *is not empty. Then, for any* $s \in \mathcal{S}$*, it holds that*

$$\|\boldsymbol{u}(t) - \boldsymbol{u}^*\| \leq \sqrt{\frac{e_2}{e_1}} e^{-e_1 \eta s (t - t_0)} \|\boldsymbol{u}(t_0) - \boldsymbol{u}^*\| + \frac{e_2(\ell_{F_J} E_J + \ell_{F_v} E_M)}{s e_1^2} \left(1 - e^{-e_1 \eta s (t - t_0)}\right), \quad (13)$$

for any initial condition $\boldsymbol{u}(t_0)$ *such that* $\|\boldsymbol{u}(t_0) - \boldsymbol{u}^*\| \leq \sqrt{\frac{e_1}{e_2}} \frac{e_1}{L}(1 - s)$. △

The proof of the result is provided in the Appendix B. The assumption that $\mathcal{S}$ is not empty is necessary to guarantee that the trajectory of $\boldsymbol{u}(t)$ never exits the region of attraction of the optimizer $\boldsymbol{u}^*$. We can notice that the first term on the right-hand-side of (13) decays over time; the second term models the effect of the measurement errors and of the errors in the computation of the Jacobian. In particular, we can notice that, as $t \to +\infty$, the right-hand side of (13) becomes

$$\lim_{t \to +\infty} \|\boldsymbol{u}(t) - \boldsymbol{u}^*\| \leq s^{-1} e_1^{-2} e_2 (\ell_{F_J} E_J + \ell_{F_v} E_M). \quad (14)$$

The asymptotic error can be reduced by increasing the accuracy in the measurement of the voltages (i.e., reducing E_M), or allocating more computational power to compute the Jacobian of the power flow equations (i.e., reducing E_J). The following result characterizes the feasibility of the solution $u(t)$.

Lemma III.6 (*Practical forward invariance*)**.** *Let the conditions in Theorem III.5 be satisfied, and let* $\boldsymbol{u}(t)$, $t \geq t_0$, *be the unique trajectory of* (9)*, and* $\boldsymbol{\nu}(t)$ *be the corresponding voltage magnitudes. Define the set*

$$\mathcal{F}_e := \{\boldsymbol{u} : \boldsymbol{u} \in \mathcal{U}, \underline{V}_e \leq H_i(\boldsymbol{u}; \boldsymbol{p}_l, \boldsymbol{q}_l) \leq \bar{V}_e, \forall i \in \mathcal{M}\} \quad (15)$$

with $\underline{V}_e := \underline{V} - E_M - 2E_{\hat{H}}$, $\bar{V}_e := \bar{V} + E_M + 2E_{\hat{H}}$, *and* $E_{\hat{H}} := \max_{\boldsymbol{u} \in \mathcal{U}} \|\hat{H}(\boldsymbol{u}; \boldsymbol{p}_l, \boldsymbol{q}_l) - H(\boldsymbol{u}; \boldsymbol{p}_l, \boldsymbol{q}_l)\|$*. Then, the feedback-based SGF* (9) *renders a set* $\mathcal{F}_s$*, with* $\mathcal{F} \subseteq \mathcal{F}_s \subseteq \mathcal{F}_e$*, forward invariant.* □

The proof is provided in Appendix C. Lemma III.6 establishes forward invariance of a set $\mathcal{F}_s$, which is a subset of $\mathcal{F}_e$ and an inflation of $\mathcal{F}$ (more details about $\mathcal{F}_s$ are provided in the proof); clearly, $\mathcal{F}_e$ tends to the set $\mathcal{F}$ with the decreasing of the error in the computation of the Jacobian and the measurement errors, which implies that $\mathcal{F}_s$ tends to $\mathcal{F}$ too. If these errors are small, the voltage violation is practically negligible.

In the case of no errors in the measurements and in the computation of the Jacobian, we have the following results.

Corollary III.7 (*Error-free implementation*)**.** *Let all the conditions in Theorem III.5 be satisfied, and assume that there are no measurement errors, i.e.,* $E_M = 0$*, and no errors in the Jacobian, i.e.,* $E_J = 0$ *and. Let* $\boldsymbol{u}(t)$, $t \geq t_0$, *be the unique trajectory of* (7)*. Then it holds that*

$$\|\boldsymbol{u}(t) - \boldsymbol{u}^*\| \leq \sqrt{\frac{e_2}{e_1}} \|\boldsymbol{u}(t_0) - \boldsymbol{u}^*\| e^{-e_1 \eta s (t - t_0)}$$

and $\lim_{t \to +\infty} \|\boldsymbol{u}(t) - \boldsymbol{u}^*\| = 0$. △

Lemma III.8 (*Forward invariance in error-free implementation*)**.** *Let the conditions in Theorem III.5 be satisfied, and assume that there are no measurement errors (i.e.,* $E_M = 0$*). Let* $\boldsymbol{u}(t)$, $t \geq t_0$, *be the unique trajectory of* (7)*, and* $\boldsymbol{\nu}(t)$ *be the corresponding trajectory of the voltages. Then,* (7) *renders the set* $\mathcal{F}$ *forward-invariant. In particular: (i) if* $\nu_i(t_0) \in [\underline{V}, \bar{V}]$*, then* $\nu_i(t) \in [\underline{V}, \bar{V}]$ *for all* $t \geq t_0$*; (ii) if* $\nu_i(t_0) \notin [\underline{V}, \bar{V}]$*, then there exists* $t' \geq t_0$ *such that* $\nu_i(t) \in [\underline{V}, \bar{V}]$ *for all* $t \geq t'$. □

Corollary III.7 quantifies the error in the convergence to $\boldsymbol{u}^*$, and certify local exponential stability properties for the proposed method. Lemma III.8 establishes that, for the case with no measurement errors and with the exact computation of the Jacobian matrix, the proposed method ensures that voltages are satisfied anytime.

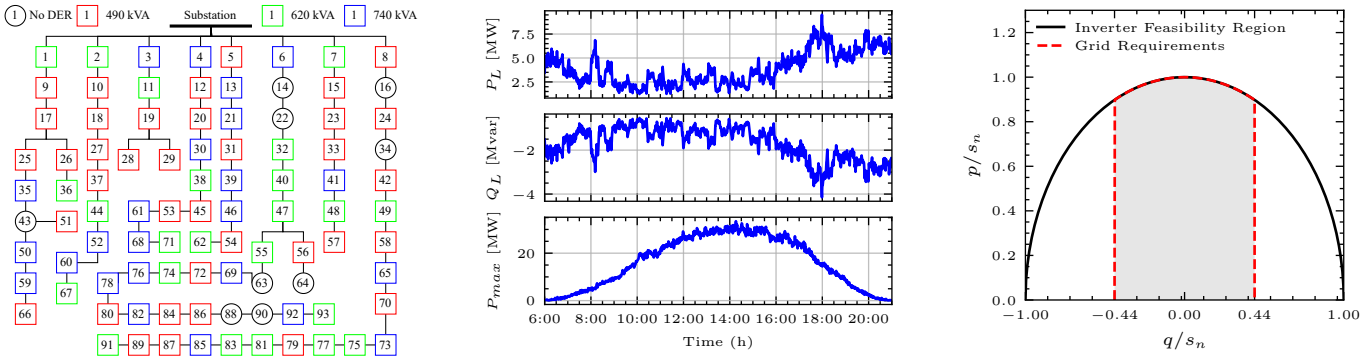

(a) (b) (c)

Fig. 2: (a) Distribution network used in the simulations. (b) Aggregated load consumption (P_L, Q_L) and PV production profiles (P_{max}) used in the simulations. (c) Operational set compared to grid code requirements inspired from the IEEE Std 1547-2018, where s_n is the inverter rated power.

C. Extension to virtual power plants

In this section, we introduce an extension of our formulation for virtual power plants (VPPs). In this case, the goal is to coordinate the operation of the DERs to regulate voltages and to provide ancillary services to the bulk power system. In particular, the coordination is to ensure that the active and reactive powers at the substation track a reference $\{P_{0,set}, Q_{0,set}\}$.

Using an expression for the powers at the substation such as $p_0 = G_p(\boldsymbol{u}; \boldsymbol{p}_l, \boldsymbol{q}_l)$ and $q_0 = G_q(\boldsymbol{u}; \boldsymbol{p}_l, \boldsymbol{q}_l)$, the OPF problem in (4) can be extended to include constraints of the form $|(G_p(\boldsymbol{u}; \boldsymbol{p}_l, \boldsymbol{q}_l) - P_{0,set})| \leq E_p$ and $|(G_q(\boldsymbol{u}; \boldsymbol{p}_l, \boldsymbol{q}_l) - Q_{0,set})| \leq E_q$, where $E_p > 0$ and $E_q > 0$ are tolerable tracking errors for the setpoints $P_{0,set}$, $Q_{0,set}$, respectively. As an additional example, one can consider the constraint:

$$\left\| \begin{bmatrix} G_p(\boldsymbol{u}; \boldsymbol{p}_l, \boldsymbol{q}_l) \\ G_q(\boldsymbol{u}; \boldsymbol{p}_l, \boldsymbol{q}_l) \end{bmatrix} - \begin{bmatrix} P_{0,set} \\ Q_{0,set} \end{bmatrix} \right\| \leq E \tag{16}$$

with $E > 0$ again a given tracking error. In the proposed measurement-based SGF, the maps $G_p(\boldsymbol{u}; \boldsymbol{p}_l, \boldsymbol{q}_l)$ and $G_q(\boldsymbol{u}; \boldsymbol{p}_l, \boldsymbol{q}_l)$ would be replaced by measurements of the active and reactive powers at the substation, respectively. Moreover, the Jacobian matrix of $G_p(\boldsymbol{u}; \boldsymbol{p}_l, \boldsymbol{q}_l)$ and $G_q(\boldsymbol{u}; \boldsymbol{p}_l, \boldsymbol{q}_l)$ with respect to $\boldsymbol{u}$ can be approximated by using a linear model [31].

IV. Numerical Experiments

We consider the medium voltage network (20 kV) shown in Fig. 2a. We used a modified network from [24], in which photovoltaic power (PV) plants have been randomly placed, with inverter-rated size picked randomly among $\{490, 620, 740\}$ kVA. Fig. 2b shows the aggregated loads and maximum available active power for PV plants throughout the day. The data is from the Open Power System Data[2], and have been modified to match the initial loads and PV plants nominal values present in the network. The reactive power demand is set such that the power factor is 0.9 (lagging). This would represent a typical summer day, with high PV production. We will show that, under these conditions, the electrical distribution network would undergo overvoltages.

[2]Data available at https://data.open-power-system-data.org/household_data/2020-04-15

A. Simulation setup

We compare the proposed measurement-based SGF with: (i) no control (NC); (ii) the online primal-dual method (PDM) proposed in [8]; and, (iii) a Volt/Var control (VVC). We also compute the solution of a batch optimization (BO) method, which is solved via the nonlinear branch flow model [35].

a) Simulation parameters: The voltage service limits $\bar{V}$ and $\underline{V}$ are set to 1.05 and 0.95 p.u., respectively. The load and PV production profiles have a granularity of 10 seconds, i.e., active/reactive power consumption and maximum available active power for PV plants change every 10 seconds. For the SGF, it means that every 10 seconds, we pursue a new optimal solution. The SGF (using a forward Euler discretization), PDM and VVC algorithms are run every second.

Based on the IEEE standard IEEE Std 1547-2018, we consider the feasible set for the PV plants shown in Fig. 2c. Although the inverter feasible set consists of a semicircle, there is no interest for PV owners to operate the PV plant at low power factors, i.e., large reactive power absorption/consumption and low active power production. Usually, PV plants are operated at unity power factor, i.e., on the vertical line passing through 0. The distribution system operator (DSO) often imposes grid requirements when a PV plant is connected to its network in order to provide support if needed. The grid requirements vary from one DSO to another. In this paper, we consider that the maximum reactive power the inverter can produce/consume is set to 44% of its nominal apparent power. The vector-valued function modelling power limits is therefore

$$\ell_i(p_i, q_i) = \begin{bmatrix} p_i^2 + q_i^2 - s_{n,i}^2 \\ p_i - p_{\max,i} \\ -p_i \\ -0.44 s_{n,i} - q_i \\ q_i - 0.44 s_{n,i} \end{bmatrix}. \tag{17}$$

Finally, we consider the following cost function for the SGF, PDM, and BO:

$$C_P(\boldsymbol{u}) = \sum_{i \in \mathcal{G}} c_p \left(\frac{s_{n,i} - p_i}{s_{n,i}} \right)^2 + c_q \left(\frac{q_i}{s_{n,i}} \right)^2 \tag{18}$$

in an effort to minimize active power curtailment and inverter power losses, with $c_p = 3$ and $c_q = 1$.

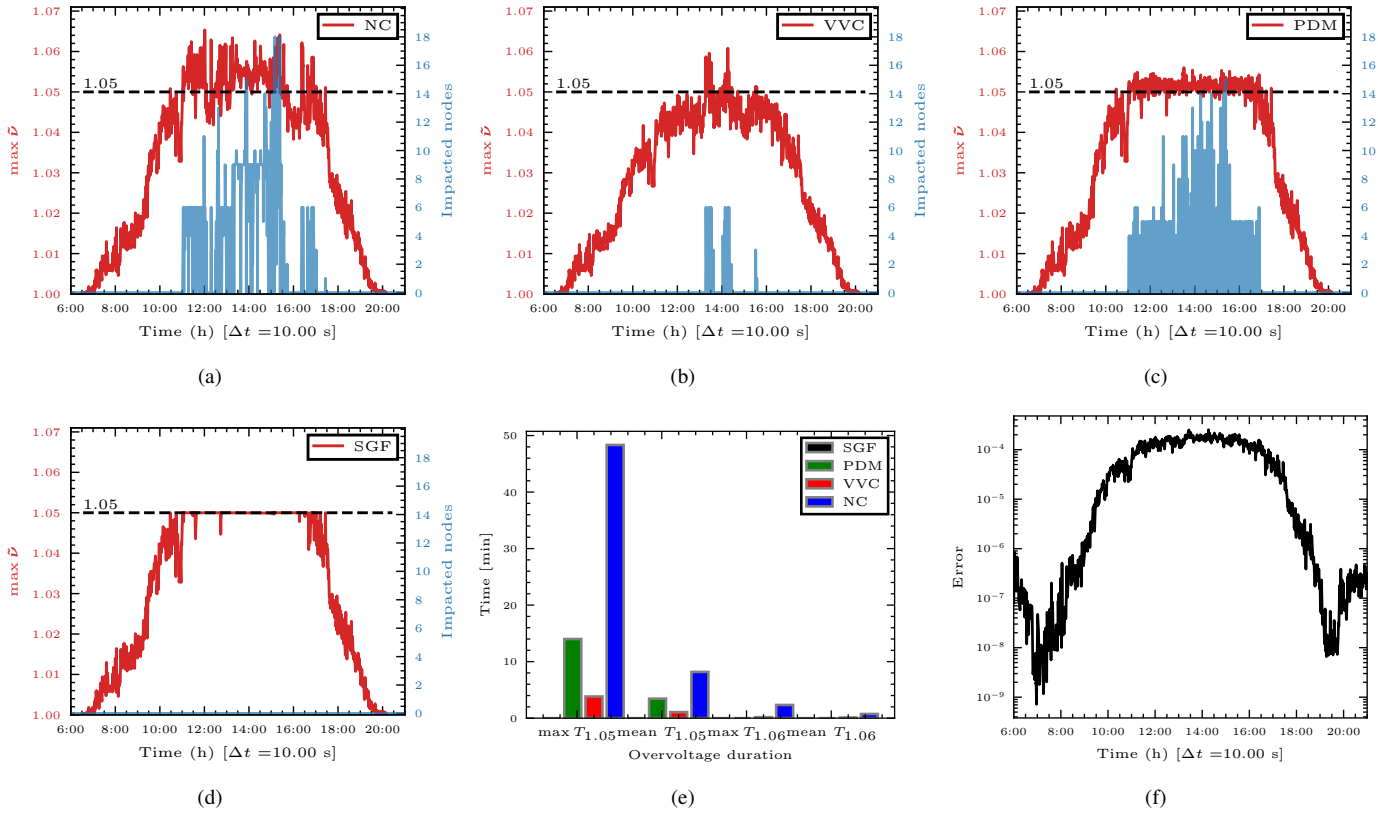

Fig. 3: (a) Overvoltages for NC. (b) Overvoltages for VVC. (c) Overvoltages for PDM. (d) Overvoltages for SGF. (e) Overvoltage duration times. (f) Linear map error: $||\tilde{H}(\boldsymbol{u};\boldsymbol{p}_l,\boldsymbol{q}_l) - H(\boldsymbol{u};\boldsymbol{p}_l,\boldsymbol{q}_l)||^2$, where $\boldsymbol{u}$ is picked from the SGF algorithm.

b) Volt/Var control and overvoltage protection scheme: The Volt/Var control is inspired by the IEEE standard IEEE Std 1547-2018. The parameters of the Volt/Var control have been adapted to match the voltage service limits considered in this paper. The maximum reactive power consumed/absorbed is set to 44% of the nominal apparent power of the PV plant. The maximum power absorbed/produced is reached for voltages 1.05/0.95 pu, respectively. Finally, we implemented a deadband for voltages between 0.99 and 1.01 pu.

c) No control: For the no-control test case, we consider an overvoltage protection of PV plants, i.e., the plant is disconnected if the voltage level is too high. We consider three different status for the PV plant: *running*, *idling*, and *disconnected*. When the PV plant is in status *idling* or *disconnected*, it does not inject active power or provide reactive power compensation. The disconnection scheme is inspired from the CENELEC EN50549-2 standard, and has been adapted considering the voltage service limits used in this paper. The PV plant changes status from *running* to *disconnected* if: (i) the voltage at the point of connection goes above 1.06 pu, (ii) the root mean square value of the voltages measured at the point of connection for the past 10 minutes goes above 1.05 pu (the voltages are measured every ten seconds).

The PV plant switches to status *idling* if the voltage at the point of connection stays below 1.05 pu for 1 minute. To switch back to *running* status, the PV plant has to be in *idling* status. The switching to *running* status occurs randomly in the interval $[1\text{min}, 10\text{min}]$ (random, uniformly distributed).

B. Results

In the following, we compare the different methods in terms of their cost function values, the system losses, and the voltage levels. Notice that system losses are not integrated in the cost function (18), since they conflict with the term that considers active power curtailment. In this paper, we design the cost function to promote renewable energy resources, hence maximizing the solar production while keeping voltage levels within pre-defined bounds. However, the DSO is also concerned by the system losses. Thus, one needs to look how the different methods perform with respect to them.

a) Voltage regulation: In Fig. 3, one can see the maximum voltage observed at every time step, as well as the number of impacted nodes where we observed a voltage greater than $\bar{V}$. It can be seen that only the SGF method does not lead to voltage violations. VVC performs well, although as shown hereafter, it leads to larger system losses and a greater cumulative cost than SGF or PDM. The overall voltage profile is also shifted downward due to its proportional feedback control. One can observe the spikes in the NC method due to multiple disconnections of DERs because of a prolonged overvoltage duration. Finally, one can see that with PDM, the voltages oscillate around the threshold voltage of 1.05 pu.

b) Over-voltage duration: In Fig. 3e, we show the duration of overvoltages. We define $T_{\geq\alpha;i}$ as a vector containing the number of consequent time steps during which node i sees his voltage above the value α. The value $\max T_{\geq\alpha}$ corresponds to the maximum value among all $T_{\geq\alpha;i}$ for $i \in \mathcal{N}$ and

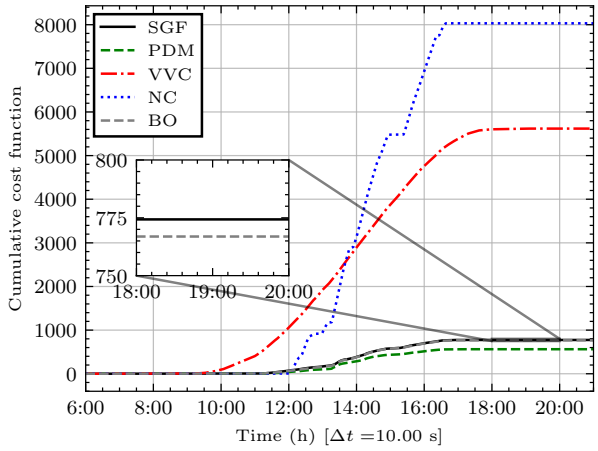

Fig. 4: Achieved values of cumulative cost (18).

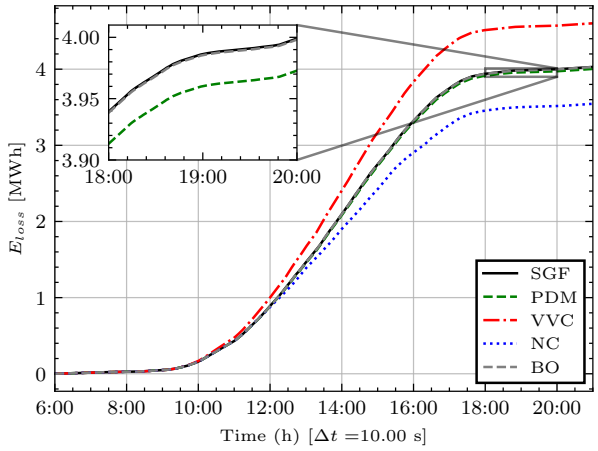

Fig. 5: Sum of energy losses throughout the day

corresponds to the maximum consequent time duration during which one nodal voltage was above α. The value mean $T_{\geq\alpha}$ is the maximum of the mean absolute values of every vector $T_{\geq\alpha;i}$ for $i \in \mathcal{N}$, representing the average time duration of overvoltage. Since SGF algorithm does not yield overvoltages, it does not appear on this graph. One can see that the NC method does not perform well, as the active power curtailment is activated only for large overvoltage (above 1.06pu) or for prolonged overvoltage (above 1.05pu).

c) Achieved cost: We show the cumulative cost function in Fig. 4, i.e., the cumulative sum of the cost function at every time step. It is clear that the NC method leads to the largest cumulative costs, as its implementation leads to full curtailment of solar production and no usage of reactive power. The VVC shows the second highest cost because of its inefficient usage of reactive power reserves. We have to bear in mind that these two solutions cannot practically achieve the optimal solutions of the BO method since they can only play with either the active or reactive power output of solar inverters. Furthermore, they are, by design, decentralized control algorithms, and do not have full information of the system state. We observe that PDM has the lowest cumulative cost, which comes at the detriment of voltage violations, as observed in Fig. 3c. The SGF cumulative cost superposes the BO cost.

d) System losses: The cumulative system losses for the different methods are shown in Fig. 5. The NC method leads to the lowest system losses as it drastically reduces the amount of active power flows in the network by fully curtailing solar production. The VVC leads to the highest system losses as it over-uses reactive power compensation to mitigate voltage issues. This results in larger power flows throughout the network, hence larger power system losses. We can observe that PDM, SGF, and BO have similar system losses.

Finally, Fig. 3f shows the error between the linear approximation of the power flow equations and the non-linear power flow equations, validating our choice for the linear map.

V. Conclusions

This paper has addressed the problem of continuously adjusting the power outputs of DERs to pursue feasible solutions of AC OPF problems. We have employed a continuous approximation of projected gradient flows, modified to accommodate voltage measurements from the electrical network, to ensure the satisfaction of voltage constraints at all times. We showed practical exponential stability for scenarios where voltage measurements are subject to errors, and where only an approximation of the Jacobian matrix of the power flow equations is available. Our method was experimentally validated on a 93-bus distribution system with realistic load and production profiles. Our approach exhibited a performance significantly superior in terms of voltage regulation to existing online primal-dual methods and Volt/VAr strategies. Future research efforts will look at data-driven implementations and event-triggered implementations of the feedback-based safe gradient flow.

Appendix

A. CBF-based design principles

In this section, we provide insights on the CBF-based design approach for the proposed measurement-based SGF. Consider rewriting the OPF problem defined in (4) in the following general form:

$$\begin{aligned} \min_{x\in\mathbb{R}^{2G}} \quad & f(x) \\ \text{s.t.} \quad & g(x) \leq 0 \end{aligned} \tag{19}$$

with $f : \mathbb{R}^{2G} \to \mathbb{R}$ and $g : \mathbb{R}^{2G} \to \mathbb{R}^P$, where P is the number of voltage and power constraints. Let $\mathcal{F} = \{x \in \mathbb{R}^{2G} \mid g(x) \leq 0\}$ and x^* be a local optimizer of (19). This point, along with the optimal dual variables $y^* \in \mathbb{R}^P$, satisfy the *Karush-Kuhn-Tucker* conditions:

$$\begin{aligned} \nabla f(x^*) + \frac{\partial g(x^*)}{\partial x}^\top y^* = 0 \\ g(x^*) \leq 0 \\ y^* \geq 0,\ (y^*)^\top g(x^*) = 0 \end{aligned} \tag{20}$$

As proposed in [23], the optimization problem (19) can be solved using nonlinear dynamics of the form:

$$\dot{x} = -\nabla f(x) - \frac{\partial g(x)}{\partial x}^\top y \tag{21}$$

which can be interpreted as a modification of the gradient flow $-\nabla f(x)$, where the input y can be designed to ensure that the set $\mathcal{F}$ is forward invariant. To this end, define the following admissible set for y:

$$K_\beta(x) := \Big\{ y \in \mathbb{R}^P_{\geq 0} \Big| - \frac{\partial g}{\partial x}\frac{\partial g}{\partial x}^\top y \leq \frac{\partial g}{\partial x}\nabla f(x) - \beta g(x) \Big\}, \tag{22}$$

where $\beta > 0$ is a design parameter, which is inspired by CBF arguments [22]; see [23]. Since we want the drift term $\frac{\partial g(x)^\top}{\partial x} y$ as small as possible while ensuring that the set $\mathcal{F}$ is feasible, the input is computed as [23]:

$$y(x) = \arg \min_{y \in K_\beta(x)} \left\| \frac{\partial g(x)^\top}{\partial x} y \right\|^2 \tag{23}$$

for each x. The overall modified gradient flow is then given by (21) with the input $y(x)$ in (23).

In [23], it is shown that (21) with the input $y(x)$ in (23) is equivalent to dynamics of the form $\dot{x} = F_\beta(x)$, where the flow $F_\beta(x)$ is defined as:

$$\begin{aligned} F_\beta(x) := \arg \min_{\theta \in \mathbb{R}^{2G}} \quad & \frac{1}{2}\left\|\theta + \nabla f(x)\right\|^2 \\ \text{s.t.} \quad & \frac{\partial g(x)}{\partial x}^\top \theta \leq -\beta g(x) \end{aligned} \tag{24}$$

In this paper, we leverage dynamics of the form (24) to solve our AC OPF problem; however, as explained in Section III, the dynamics are modified to accommodate measurements.

B. Proof of Theorem III.5

We recall that $\boldsymbol{\nu}$ is a short-hand notation for the real voltages, i.e., $\boldsymbol{\nu} = H(\boldsymbol{u}; \boldsymbol{p}_l, \boldsymbol{q}_l)$, and $\tilde{\boldsymbol{\nu}}$ is the vector of (pseudo-)measurements. Recall also that $F_\beta(\boldsymbol{u}, \boldsymbol{\nu}) = \bar{F}_\beta(\boldsymbol{u}, \mathbb{0}, \mathbb{0})$ and $\hat{F}_\beta(\boldsymbol{u}, \tilde{\boldsymbol{\nu}}) = \bar{F}_\beta(\boldsymbol{u}, J_{\hat{H}}(\boldsymbol{u}) - J_H(\boldsymbol{u}), \tilde{\boldsymbol{\nu}} - \boldsymbol{\nu})$. First, we express our controller as:

$$\begin{aligned} \dot{\boldsymbol{u}} &= \eta \hat{F}_\beta(\boldsymbol{u}, \tilde{\boldsymbol{\nu}}) \\ &= \eta \bar{F}_\beta(\boldsymbol{u}, \mathbb{0}, \mathbb{0}) \\ &\quad + \eta[\bar{F}_\beta(\boldsymbol{u}, J_{\hat{H}}(\boldsymbol{u}) - J_H(\boldsymbol{u}), \tilde{\boldsymbol{\nu}} - \boldsymbol{\nu}) - \bar{F}_\beta(\boldsymbol{u}, \mathbb{0}, \tilde{\boldsymbol{\nu}} - \boldsymbol{\nu})] \\ &\quad + \eta[\bar{F}_\beta(\boldsymbol{u}, \mathbb{0}, \tilde{\boldsymbol{\nu}} - \boldsymbol{\nu}) - \bar{F}_\beta(\boldsymbol{u}, \mathbb{0}, \mathbb{0})] \end{aligned}$$

where we added and subtracted $\bar{F}_\beta(\boldsymbol{u}, \mathbb{0}, \mathbb{0})$ and $\bar{F}_\beta(\boldsymbol{u}, \mathbb{0}, \tilde{\boldsymbol{\nu}} - \boldsymbol{\nu})$, and we re-organized the terms. The feedback-based SGF can then be understood as a perturbation of the nominal gradient flow $\bar{F}_\beta(\boldsymbol{u}, \mathbb{0}, \mathbb{0})$.

By [23, Lemma 5.11 and Theorem 5.6(iii)], $\bar{F}_\beta(\boldsymbol{u}, \mathbb{0}, \mathbb{0})$ is differentiable at $\boldsymbol{u}^*$ and its Jacobian $E = \frac{\partial \bar{F}_\beta(\boldsymbol{u}, \mathbb{0}, \mathbb{0})}{\partial \boldsymbol{u}} \big|_{\boldsymbol{u}=\boldsymbol{u}^*}$ is negative definite. Recall that $e_1 = -\lambda_{\max}(E)$ and $e_2 = -\lambda_{\min}(E)$. Let $P := \int_0^\infty (\exp(E\zeta)^\top \exp(E\zeta) d\zeta$, and then by [34, Theorem 4.12], it holds that $PE + E^\top P = -\mathbf{I}_n$, and $\frac{1}{2e_2}\|u - u^*\|_2^2 \leq (u - u^*)^\top P (u - u^*) \leq \frac{1}{2e_1}\|u - u^*\|_2^2$. Let $V_1(\boldsymbol{u}) := (\boldsymbol{u} - \boldsymbol{u}^*)^\top P (\boldsymbol{u} - \boldsymbol{u}^*)$; then we bound $2(\boldsymbol{u} - \boldsymbol{u}^*)^\top P \bar{F}_\beta(\boldsymbol{u}, \mathbb{0}, \mathbb{0})$ and then leverage this bound to estimate $\dot{V}_1$:

$$\begin{aligned} &2(\boldsymbol{u} - \boldsymbol{u}^*)^\top P \bar{F}_\beta(\boldsymbol{u}, \mathbb{0}, \mathbb{0}) \\ &\quad = (\boldsymbol{u} - \boldsymbol{u}^*)^\top \left(PE + E^\top P\right)(\boldsymbol{u} - \boldsymbol{u}^*) \\ &\qquad + 2(\boldsymbol{u} - \boldsymbol{u}^*)^\top P \hat{g}(\boldsymbol{u}) \\ &\quad \leq -\|\boldsymbol{u} - \boldsymbol{u}^*\|^2 + \frac{1}{e_1}\|\boldsymbol{u} - \boldsymbol{u}^*\| L \|\boldsymbol{u} - \boldsymbol{u}^*\|^2 \\ &\quad \leq \left(-1 + \frac{L}{e_1}\|\boldsymbol{u} - \boldsymbol{u}^*\|_2\right)\|\boldsymbol{u} - \boldsymbol{u}^*\|_2^2 \leq -s\|\boldsymbol{u} - \boldsymbol{u}^*\|^2 \end{aligned}$$

where the last inequality holds if $\|\boldsymbol{u} - \boldsymbol{u}^*\| \leq \frac{e_1}{L}(1 - s)$, for any $s \in (s_{\min}, 1]$. Then,

$$\begin{aligned} \dot{V}_1 &= 2(\boldsymbol{u} - \boldsymbol{u}^*)^\top P \dot{u} \\ &\quad = 2\eta(\boldsymbol{u} - \boldsymbol{u}^*)^\top P \bar{F}_\beta(\boldsymbol{u}, \mathbb{0}, \mathbb{0})) \\ &\quad + 2\eta(\boldsymbol{u} - \boldsymbol{u}^*)^\top P[\bar{F}_\beta(\boldsymbol{u}, J_{\hat{H}} - J_H, \tilde{\boldsymbol{\nu}} - \boldsymbol{\nu}) - \bar{F}_\beta(\boldsymbol{u}, \mathbb{0}, \tilde{\boldsymbol{\nu}} - \boldsymbol{\nu})] \\ &\quad + 2\eta(\boldsymbol{u} - \boldsymbol{u}^*)^\top P[\bar{F}_\beta(\boldsymbol{u}, \mathbb{0}, \tilde{\boldsymbol{\nu}} - \boldsymbol{\nu}) - \bar{F}_\beta(\boldsymbol{u}, \mathbb{0}, \mathbb{0})] \\ &\quad \leq -\eta s\|\boldsymbol{u} - \boldsymbol{u}^*\|^2 + 2\eta\ell_{F_J}\|\boldsymbol{u} - \boldsymbol{u}^*\|\|P\|\|J_H - J_{\hat{H}}\| \\ &\quad + 2\eta\ell_{F_v}\|\boldsymbol{u} - \boldsymbol{u}^*\|\|P\|\|\tilde{\boldsymbol{\nu}} - \boldsymbol{\nu}\| \\ &\quad \leq -\eta s\|\boldsymbol{u} - \boldsymbol{u}^*\|^2 + \eta\frac{\ell_{F_J}E_J + \ell_{F_v}E_M}{e_1}\|\boldsymbol{u} - \boldsymbol{u}^*\| \\ &\quad \leq -2e_1\eta s V_1 + \eta\sqrt{2e_2}\frac{\ell_{F_J}E_J + \ell_{F_v}E_M}{e_1}\sqrt{V_1}. \end{aligned}$$

Define $V_2(\boldsymbol{u}) := \sqrt{V_1(\boldsymbol{u})}$. Then,

$$\begin{aligned} \dot{V}_2 = \frac{\dot{V}_1}{2\sqrt{V_1}} &\leq \frac{-2e_1\eta s V_1 + \eta\sqrt{2e_2}\frac{\ell_{F_J}E_J + \ell_{F_v}E_M}{e_1}\sqrt{V_1}}{2\sqrt{V_1}} \\ &= -e_1\eta s V_2 + \eta\sqrt{2e_2}\frac{\ell_{F_J}E_J + \ell_{F_v}E_M}{2e_1} \end{aligned}$$

In addition, we note that that for any $a \geq 0,\ b > 0$, $y(t) = y(t_0)\exp(-b(t - t_0)) + \frac{a}{b}(1 - \exp(-b(t - t_0))$ is the solution of $\dot{y} = -by + a, y(t_0) = y(t_0)$. Hence by the Comparison Lemma [34, Lemma 3.4], it follows that

$$\begin{aligned} V_2(t) &\leq V_2(t_0)e^{-e_1\eta s(t - t_0)} \\ &\quad + \frac{\sqrt{2e_2}(\ell_{F_J}E_J + \ell_{F_v}E_M)}{2se_1^2}\left(1 - e^{-e_1\eta s(t - t_0)}\right). \end{aligned}$$

Thus, one has that

$$\begin{aligned} \|\boldsymbol{u}(t) - \boldsymbol{u}^*\| &\leq \sqrt{2e_2}V_2(t) \\ &\leq \sqrt{2e_2}V_2(t_0)e^{-e_1\eta s(t - t_0)} \\ &\quad + \frac{2e_2(\ell_{F_J}E_J + \ell_{F_v}E_M)}{2se_1^2}\left(1 - e^{-e_1\eta s(t - t_0)}\right) \\ &\leq \sqrt{\frac{1}{2e_1}}\sqrt{2e_2}e^{-e_1\eta s(t - t_0)}\|\boldsymbol{u}(t_0) - \boldsymbol{u}^*\| \\ &\quad + \frac{e_2(\ell_{F_J}E_J + \ell_{F_v}E_M)}{se_1^2}\left(1 - e^{-e_1\eta s(t - t_0)}\right) \\ &= \sqrt{\frac{e_2}{e_1}}e^{-e_1\eta s(t - t_0)}\|\boldsymbol{u}(t_0) - \boldsymbol{u}^*\| \\ &\quad + \frac{e_2(\ell_{F_J}E_J + \ell_{F_v}E_M)}{se_1^2}\left(1 - e^{-e_1\eta s(t - t_0)}\right). \end{aligned}$$

which proves the result. The limits for $t \to +\infty$ can be computed straightforwardly.

C. Proof of Lemma III.6

The proof leverages Nagumo's Theorem [36]. For the feedback-based SGF $\hat{F}_\beta(\boldsymbol{u}, \boldsymbol{\nu})$ in (9), it holds that $-\nabla \hat{H}_i(\boldsymbol{u})^\top \hat{F}_\beta \leq -\beta\,(\underline{V} - \tilde{\nu}_i)$. Recall that $\tilde{\nu}_i = H(\boldsymbol{u}; \boldsymbol{p}_l, \boldsymbol{q}_l) + e_i$, for $i \in \mathcal{M}$. It follows that

$$
\begin{aligned}
&-\nabla \hat{H}_i(\boldsymbol{u})^\top \hat{F}_\beta \leq -\beta\,(\underline{V} - H(\boldsymbol{u}; \boldsymbol{p}_l, \boldsymbol{q}_l) - e_i) \\
&= -\beta(\underline{V} - \hat{H}(\boldsymbol{u}; \boldsymbol{p}_l, \boldsymbol{q}_l) - e_i + (H(\boldsymbol{u}; \boldsymbol{p}_l, \boldsymbol{q}_l) - \hat{H}(\boldsymbol{u}; \boldsymbol{p}_l, \boldsymbol{q}_l))) \\
&\leq -\beta((\underline{V} - E_M - E_{\hat{H}}) - \hat{H}(\boldsymbol{u}; \boldsymbol{p}_l, \boldsymbol{q}_l))
\end{aligned}
$$

where $E_{\hat{H}} := \max_{\boldsymbol{u} \in \mathcal{U}} \|H(\boldsymbol{u}; \boldsymbol{p}_l, \boldsymbol{q}_l) - \hat{H}(\boldsymbol{u}; \boldsymbol{p}_l, \boldsymbol{q}_l)\|$. Similarly, it also holds that $\nabla \hat{H}_i(\boldsymbol{u})^\top \hat{F}_\beta \leq -\beta(\hat{H}(\boldsymbol{u}; \boldsymbol{p}_l, \boldsymbol{q}_l) - (\bar{V} + E_M + E_{\hat{H}}))$. Thus, the set

$$
\begin{aligned}
\mathcal{F}_s :=\{&\boldsymbol{u} : \underline{V} - E_M - E_{\hat{H}} \leq \hat{H}_i(\boldsymbol{u}; \boldsymbol{p}_l, \boldsymbol{q}_l) \leq \bar{V} + E_M + E_{\hat{H}}, \\
&\forall i \in \mathcal{M}, \boldsymbol{u} \in \mathcal{U}\}
\end{aligned}
$$

is forward invariant under (9). Note that $\mathcal{F}_s$ is a subset of $\mathcal{F}_e$, and this concludes the proof.

REFERENCES

[1] J. A. Taylor, S. V. Dhople, and D. S. Callaway, "Power systems without fuel," *Renewable and Sustainable Energy Reviews*, vol. 57, pp. 1322–1336, 2016.

[2] B. Kroposki, A. Bernstein, J. King, D. Vaidhynathan, X. Zhou, C.-Y. Chang, and E. Dall'Anese, "Autonomous energy grids: Controlling the future grid with large amounts of distributed energy resources," *IEEE Power and Energy Magazine*, vol. 18, no. 6, pp. 37–46, 2020.

[3] Y. Zhu and K. Tomsovic, "Optimal distribution power flow for systems with distributed energy resources," *International Journal of Electrical Power & Energy Systems*, vol. 29, no. 3, pp. 260–267, 2007.

[4] F. Capitanescu, "Critical review of recent advances and further developments needed in AC optimal power flow," *Electric Power Systems Research*, vol. 136, pp. 57–68, 2016.

[5] K. Baker, "Emulating AC OPF solvers for obtaining sub-second feasible, near-optimal solutions," *arXiv preprint arXiv:2012.10031*, 2020.

[6] R. Nellikkath and S. Chatzivasileiadis, "Physics-informed neural networks for AC optimal power flow," *Electric Power Systems Research*, vol. 212, p. 108412, 2022.

[7] S. Bolognani, R. Carli, G. Cavraro, and S. Zampieri, "Distributed reactive power feedback control for voltage regulation and loss minimization," *IEEE Transactions on Automatic Control*, vol. 60, no. 4, pp. 966–981, 2014.

[8] E. Dall'Anese and A. Simonetto, "Optimal power flow pursuit," *IEEE Transactions on Smart Grid*, vol. 9, no. 2, pp. 942–952, 2016.

[9] A. Hauswirth, S. Bolognani, G. Hug, and F. Dorfler, "Projected gradient descent on Riemannian manifolds with applications to online power system optimization," in *54th Annual Allerton Conference on Communication, Control, and Computing*, Sept 2016, pp. 225–232.

[10] A. Hauswirth, A. Zanardi, S. Bolognani, G. Hug, and F. Dorfler, "Online optimization in closed loop on the power flow manifold," in *IEEE PES PowerTech conference*, 2017.

[11] S. Nowak, Y. C. Chen, and L. Wang, "A measurement-based gradient-descent method to optimally dispatch DER reactive power," in *IEEE Photovoltaic Specialists Conference*. IEEE, 2020.

[12] L. Ortmann, C. Rubin, A. Scozzafava, J. Lehmann, S. Bolognani, and F. Dörfler, "Deployment of an online feedback optimization controller for reactive power flow optimization in a distribution grid," *arXiv preprint arXiv:2305.06702*, 2023.

[13] Z. Yuan, G. Cavraro, M. K. Singh, and J. Cortés, "Learning provably stable local Volt/Var controllers for efficient network operation," *IEEE Transactions on Power Systems*, 2023, to appear.

[14] A. Bernstein and E. Dall'Anese, "Real-time feedback-based optimization of distribution grids: A unified approach," *IEEE Transactions on Control of Network Systems*, vol. 6, no. 3, pp. 1197–1209, 2019.

[15] Y. Chen, A. Bernstein, A. Devraj, and S. Meyn, "Model-free primal-dual methods for network optimization with application to real-time optimal power flow," in *American Control Conference*, 2020, pp. 3140–3147.

[16] J. C. Olives-Camps, Á. R. del Nozal, J. M. Mauricio, and J. M. Maza-Ortega, "A model-less control algorithm of DC microgrids based on feedback optimization," *International Journal of Electrical Power & Energy Systems*, vol. 141, p. 108087, 2022.

[17] L. Gan and S. H. Low, "An online gradient algorithm for optimal power flow on radial networks," *IEEE Journal on Selected Areas in Communications*, vol. 34, no. 3, pp. 625–638, 2016.

[18] A. Bernstein, L. Reyes-Chamorro, J.-Y. Le Boudec, and M. Paolone, "A composable method for real-time control of active distribution networks with explicit power setpoints. part I: Framework," *Electric Power Systems Research*, vol. 125, pp. 254–264, 2015.

[19] Y. Tang, K. Dvijotham, and S. Low, "Real-time optimal power flow," *IEEE Trans. on Smart Grid*, vol. 8, no. 6, pp. 2963–2973, 2017.

[20] J.-L. Lupien, I. Shames, and A. Lesage-Landry, "Online interior-point methods for time-varying equality-constrained optimization," *arXiv preprint arXiv:2307.16128*, 2023.

[21] A. Colot, T. Stegen, and B. Cornélusse, "Fully distributed real-time voltage control in active distribution networks with large penetration of solar inverters," in *IEEE Belgrade PowerTech*, 2023.

[22] A. D. Ames, S. Coogan, M. Egerstedt, G. Notomista, K. Sreenath, and P. Tabuada, "Control barrier functions: Theory and applications," in *European control conference*, 2019, pp. 3420–3431.

[23] A. Allibhoy and J. Cortés, "Control barrier function-based design of gradient flows for constrained nonlinear programming," *IEEE Transactions on Automatic Control*, vol. 69, no. 6, 2024.

[24] D. Sarajlić and C. Rehtanz, "Low voltage benchmark distribution network models based on publicly available data," in *IEEE PES Innovative Smart Grid Technologies Europe*, 2019.

[25] W. H. Kersting, *Distribution System Modeling and Analysis*. 2nd ed., Boca Raton, FL: CRC Press, 2007.

[26] S. Bolognani and S. Zampieri, "On the existence and linear approximation of the power flow solution in power distribution networks," *IEEE Transactions on Power Systems*, vol. 31, no. 1, pp. 163–172, 2015.

[27] A. Bernstein, C. Wang, E. Dall'Anese, J.-Y. Le Boudec, and C. Zhao, "Load flow in multiphase distribution networks: Existence, uniqueness, non-singularity and linear models," *IEEE Transactions on Power Systems*, vol. 33, no. 6, pp. 5832–5843, 2018.

[28] A. V. Fiacco, "Sensitivity analysis for nonlinear programming using penalty methods," *Mathematical programming*, vol. 10, no. 1, pp. 287–311, 1976.

[29] A. Hauswirth, S. Bolognani, G. Hug, and F. Dörfler, "Generic existence of unique lagrange multipliers in ac optimal power flow," *IEEE Control Systems Letters*, vol. 2, no. 4, pp. 791–796, 2018.

[30] G. Banjac, B. Stellato, N. Moehle, P. Goulart, A. Bemporad, and S. Boyd, "Embedded code generation using the osqp solver," in *IEEE Conference on Decision and Control*, 2017, pp. 1906–1911.

[31] S. V. Dhople, S. S. Guggilam, and Y. C. Chen, "Linear approximations to AC power flow in rectangular coordinates," in *2015 53rd Annual Allerton Conference on Communication, Control, and Computing (Allerton)*, 2015, pp. 211–217.

[32] A. Angioni, T. Schlösser, F. Ponci, and A. Monti, "Impact of pseudo-measurements from new power profiles on state estimation in low-voltage grids," *IEEE Transactions on Instrumentation and Measurement*, vol. 65, no. 1, pp. 70–77, 2015.

[33] J. Liu, "Sensitivity analysis in nonlinear programs and variational inequalities via continuous selections," *SIAM Journal on Control and Optimization*, vol. 33, no. 4, pp. 1040–1060, 1995.

[34] H. K. Khalil, "Nonlinear systems," *Patience Hall*, 2002.

[35] M. Baran and F. Wu, "Optimal capacitor placement on radial distribution systems," *IEEE Transactions on Power Delivery*, vol. 4, no. 1, pp. 725–734, 1989.

[36] M. Nagumo, "Über die lage der integralkurven gewöhnlicher differentialgleichungen," *Proceedings of the Physico-Mathematical Society of Japan. 3rd Series*, vol. 24, pp. 551–559, 1942.